Korean J Physiol Pharmacol
Vol 17: 237−243, June, 2013
http://dx.doi.org/10.4196/kjpp.2013.17.3.237

Cytotoxic Activity and Quantitative Structure Activity Relationships of Arylpropyl Sulfonamides

Yu Jin Hwang, Sang Min Park, Chul Bu Yim, and Chaeuk Im

College of Pharmacy, Chung-Ang University, Seoul 156-756, Korea

B13 is a ceramide analogue and apoptosis inducer with potent cytotoxic activity. A series of arylpropyl sulfonamide analogues of B13 were evaluated for their cytotoxicity using MTT assays in prostate cancer PC-3 and leukemia HL-60 cell lines. Some compounds (4, 9, 13, 14, 15, and 20) showed stronger activities than B13 in both tumor cell lines, and compound (15) gave the most potent activity with IC_{50} values of 29.2 and 20.7 μM, for PC-3and HL-60 cells, respectively. Three-dimensional quantitative structure-activity relationship (3D-QSAR) analysis was performed to build highly reliable and predictive CoMSIA models with cross-validated q^2 values of 0.816 and 0.702, respectively. Our results suggest that long alkyl chains and a 1R, 2R configuration of the propyl group are important for the cytotoxic activities of arylpropyl sulfonamides. Moreover, the introduction of small hydrophobic groups in the phenyl ring and sulfonamide group could increase biological activity.

Key Words: Arylpropanol, Ceramide, Cytotoxicity, QSAR

INTRODUCTION

Apoptosis is an endogenous program of cell death that is mediated through biochemical modulators, and it is induced by anticancer agents, tumor necrosis factor, and ionizing radiation [1,2]. Because ceramide is known to be a key modulator of apoptosis and its accumulation in cells leads to apoptosis, many approaches have been explored to increase endogenous ceramide [3-5]. These approaches include the application of short-chain ceramides (C_6-ceramide) [6-8] and induction of ceramide by modulation of ceramide-metabolizing enzymes (LCL 15 and LCL 16) [9-13].

In recent years, ceramide analogues have emerged as a new strategy for cancer therapy [14-17]. The ceramide analogues, such as sphingosine, sphinganine, and C_2-eramide, were known to induce apoptotic cell death in the malignant melanoma, colon cancer cells, and prostate cancer cells [18-21]. It was reported that the activity of ceramide analogues is influenced by the stereochemistry and chain length of the amide moiety. Analogues with a ceramide configuration (2S, 3R) are not active, whereas their stereoisomers inhibit cell growth. The ceramides with medium size alkyl chains (C_{11}~C_{15}) are active compounds, but ceramides with shorter (C_1~C_9) and longer (C_{17}~C_{23}) alkyl chains are less active [22]. The aromatic analogues of ceramide like D-*e*-Mapp with a 1S, 2R configuration increase endogenous ceramide to induce apoptosis in many cancer cell lines [23-26]. Another active analogue, B13 with a 1R, 2R configuration, exhibited cytotoxicity in malignant melanoma, colon, and prostate cancer cells [27-29]. B13 also induced apoptosis in cancer cells, increased the cellular ceramide level, inhibited metastasis, and had no effect on normal cells [29-31].

It has been reported that isosteric replacement of the amide group in a ceramide by urea or amine can increase the ceramidase inhibitory activity and cytotoxicity [32]. And the carboxyl moiety of ceramide can also be bioisosterically replaced by a sulfone group. Sulfonamides are known to have various biological activities, including hypoglycemic, diuretic, antibacterial activity, and cytotoxicity [33-36]. Extending these findings to the ceramide, we suspected that introduction of a phenyl ring, as in D-*e*-Mapp and B13, altering alkyl chain lengths and stereochemistry, and bioisosterical replacement of the carboxyl group with a sulfone group would improve and modify the biological properties of ceramide.

As a continuation of our previously reported work, in which arylpropyl thiourea analogues (Fig. 1) were studied [37], we determined the cytotoxic activity of 21 new arylpropyl sulfonamide analogues (Fig. 1) in prostate cancer and leukemia cell lines to evaluate the effects of R and S enantiomers in propyl moiety, a *p*-nitro group in the phenyl

Received November 22, 2012, Revised February 22, 2013, Accepted March 6, 2013

Corresponding to: Chaeuk Im, College of Pharmacy, Chung-Ang University, Heuksuk-dong, Dongjak-gu, Seoul 156-756, Korea. (Tel) 82-2-820-5603, (Fax) 82-2-816-7338, (E-mail) chaeukim@cau.ac.kr

ABBREVIATIONS: DMSO, dimethyl sulfoxide; D-*e*-Mapp, (1S,2R)-2-N-(tetradecanoylamino)-1-phenyl-1-propanol; B13, (1R,2R)-2-N-(tetradecanoylamino)-1-(4'-nitrophenyl)-1,3-propanediol; PBS, phosphate-buffered saline; MTT, 3-[4,5-dimethylthiazol-2-yl]-2,5-diphenyltetrazolium bromide; 3D-QSAR, three dimensional quantitative structure activity relationship; CoMSIA, comparative molecular similarity indices analysis.

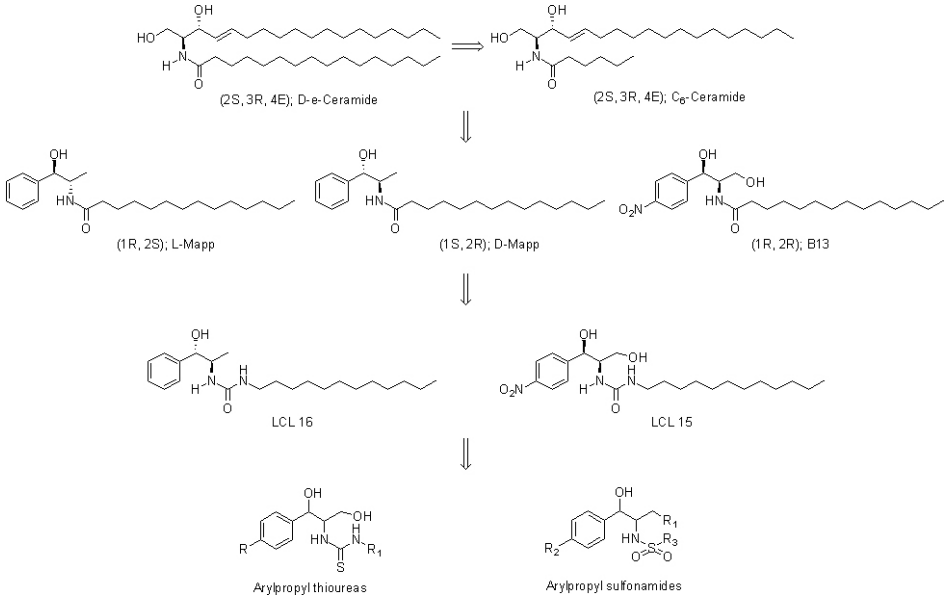

Fig. 1. Ceramide, Mapp, B13, and arylpropyl compounds.

ring, and the alkyl chain length of the sulfonamide moiety. We also perform QSAR analysis to investigate the relationship between the structural features and cytotoxicity of arylpropyl sulfonamides and to develop more potent anticancer agents.

METHODS

Materials

A series of arylpropyl compounds were previously synthesized in our lab. Phosphate-buffered saline (PBS) was purchased from Boehringer Mannheim. Dimethyl sulfoxide (DMSO), 3-[4,5-dimethylthiazol-2-yl]-2,5-diphenyltetrazolium bromide (MTT), and other reagents were obtained from Sigma.

In vitro cytotoxic assay

The cytotoxicity of arylpropyl compounds was evaluated in two human tumor cell lines: prostate cancer PC-3 cells and leukemic cancer HL-60 cells. The cytotoxicity was determined using a MTT-based colorimetric assay [38]. The cells were treated as described in the Table 1 legend and the results from the assay are shown in Table 1 [39].

Data sets

Twenty-one arylpropyl compounds with cytotoxic IC_{50} values ranging from 20.7 to 267.3 μM were used to carry out 3D-QSAR analysis. Their molecular structures are illustrated in Table 1. The test set was selected based on their various configurations at C_1 and C_2 and used for external validation of the 3D-QSAR models. The training set was consisted of seventeen compounds including B13 and the test set was made of the following four different configuration structures, compound 2(1R,2S), 8(1S,2R), 12(1R,2R), and 17(1S,2S). All IC_{50} values were transformed into pIC_{50} ($-\log IC_{50}$) values and used as the dependent variables in the CoMSIA studies.

Molecular modeling and alignment

The modeling software Sybyl-X 1.3 was used for the structure building, molecules modeling, partial least squares, and conducting CoMSIA [40]. The structures of compounds were generated with a sketch tool and energy minimization was performed using a TRIPOS force field with the Powell method and conjugate gradient termination. The atomic charges of molecules were calculated using the Gasteiger- Hückel charges. Simulated annealing was used to determine the low-energy conformations. One of the most important requirements for CoMSIA models is that the 3D structures of molecules are aligned to a suitable conformational template. The molecular alignment was achieved by the fitting atoms method. In Table 1, the bold line represents a common substructure and B13 was used as a template molecule in the alignment.

CoMSIA 3D-QSAR models

CoMSIA is based on the relationship between the biological activity and structural properties of compounds when the receptor structure is not known. It evaluates the five physicochemical properties: steric, electrostatic, hydrophobic, hydrogen bond acceptor, and hydrogen bond donor fields. The CoMSIA method involves a common probe atom and similarity indices determined in regularly spaced grid points for the aligned molecules. The common probe atom with a radius of 1.0 Å, charge of +1, hydrophobicity of +1, hydrogen bond donating of +1, and hydrogen bond accepting of +1 was used to calculate the five fields. A default value of 0.3 was used for the attenuation factor.

Partial least squares (PLS) analysis

In the PLS analysis, three CoMSIA descriptors (electrostatic, hydrophobic, and hydrogen bond acceptor fields) were used as independent variables, and the pIC_{50} values

Table 1. Structures and cytotoxic activities of arylpropyl sulfonamides

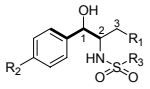

Compounds	R_1	R_2	R_3	Configuration	Cytotoxicity IC_{50} (μM)	
					Prostate cancer (PC-3)	Leukemia (HL-60)
1	H	H	C_7H_{15}	1R, 2S	189.3	129.8
2	H	H	C_8H_{17}	1R, 2S	95.3	77.6
3	H	H	C_9H_{19}	1R, 2S	81.7	53.7
4	H	H	$C_{11}H_{23}$	1R, 2S	44.9	28.5
5	H	H	$C_{13}H_{27}$	1R, 2S	45.1	34.3
6	H	H	C_7H_{15}	1S, 2R	188.5	130.4
7	H	H	C_8H_{17}	1S, 2R	80.8	62.8
8	H	H	C_9H_{19}	1S, 2R	64.3	44.9
9	H	H	$C_{11}H_{23}$	1S, 2R	40.5	33.1
10	H	H	$C_{13}H_{27}$	1S, 2R	67.8	44.4
11	OH	NO_2	C_7H_{15}	1R, 2R	98.4	116.6
12	OH	NO_2	C_8H_{17}	1R, 2R	52.8	54.9
13	OH	NO_2	C_9H_{19}	1R, 2R	31.8	27.6
14	OH	NO_2	$C_{11}H_{23}$	1R, 2R	39.1	24.7
15	OH	NO_2	$C_{13}H_{27}$	1R, 2R	29.2	20.7
16	OH	NO_2	C_7H_{15}	1S, 2S	>267.3	160.6
17	OH	NO_2	C_8H_{17}	1S, 2S	75.1	67.6
18	OH	NO_2	C_9H_{19}	1S, 2S	51.0	41.4
19	OH	NO_2	$C_{11}H_{23}$	1S, 2S	56.0	37.7
20	OH	NO_2	$C_{13}H_{27}$	1S, 2S	35.9	23.0
B13				1R, 2R	79.3	33.6

The cells were plated at a density of approximately 1×10^4 cells/well in 96-well plates. Each well contained 180 μl of medium and 20 μl of 10×concentration of prepared compounds or PBS were added. After 96 h of culture, 0.1 mg of MTT was added to each well and incubated at 37°C for 4 h. The plates were centrifuged at 450×g to precipitate the formazan crystals. The medium was rem9oved and 150 μL of DMSO was added to each well to dissolve the formazan. In this assay, MTT was converted to blue formazan by mitochondrial dehydrogenase. The intensity of the blue color was measured with a microplate reader at a wavelength of 540 nm. The measured mean values were expressed as the IC_{50}, the concentration that reduced the optical density of the treated cells by 50% with respect to the untreated controls.

Table 2. PLS analysis of CoMSIA 3D-QSAR models

PLS Statistics		Prostate cancer (PC-3)	Leukemia (HL-60)
$q^{2a)}$		0.816	0.702
$r^{2b)}$		0.999	0.997
SEE[c)]		0.009	0.018
F[d)]		3841.601	1000.475
PLS component[e)]		4	4
r^2_{pred}[f)]		0.776	0.974
Field contribution	Steric	-	-
	Electrostatic	0.416	0.518
	Hydrophobic	0.335	0.254
	H-bond donor	-	-
	H-bond acceptor	0.249	0.228

[a)]q^2, cross-validated correlation coefficient from leave-one- out (LOO); [b)]r^2, non-cross-validated correlation coefficient; [c)]SEE, standard error of estimate; [d)]F, F-test value; [e)]PLS component, optimum number of components; [f)]r^2_{pred}, predicted correlation coefficient.

were used as dependent variables. The predictive pIC_{50} values of the models were evaluated by leave-one-out (LOO) cross-validation. In the LOO method, one compound is removed from the data set and its biological activity is predicted with the model derived from the rest of data set. The LOO method determines the optimum number of components, which are then used for the non-cross-validated analysis. To test the utility of the model as a predictive tool, the test set compounds that were not used in the model generation were predicted.

RESULTS

In vitro cytotoxic activity

The cytotoxicities of 21 compounds were evaluated *in vitro* and presented in Table 1. B13 gave moderate cytotoxicity with IC_{50} values of 79.3 and 33.6 μM for prostate cancer PC-3 and leukemia HL-60 cells, respectively. The IC_{50} values of the other structures ranged from 29.2 to 267.3 μM for PC-3 cells and 20.7 to 160.6 μM for HL-60 cells.

For prostate cancer PC-3 cells, the long alkyl chain ($C_{13}H_{27}$ and $C_{11}H_{23}$) compounds (4, 5, 9, 10, 14, 15, 19, and 20) exhibited more potent activities than B13 to give IC_{50} values of 44.9, 45.1, 40.5, 67.8, 39.1, 29.2, 56, and 35.9 μM, respectively. However the short alkyl chain (C_7H_{15} and C_8H_{17}) compounds (1, 2, 6, 7, 11, and 16) showed less potent

Table 3. Residuals of the predicted cytotoxicities (pIC50) of training set

Compounds	Prostate cancer cells (PC-3 cells)			Leukemia cells (HL-60 cells)		
	Experimental[a)]	Predicted[b)]	Residual[c)]	Experimental[a)]	Predicted[b)]	Residual[c)]
1	3.72	3.74	−0.02	3.89	3.85	0.03
3	4.09	4.08	0.01	4.27	4.27	0.00
4	4.35	4.34	0.01	4.55	4.55	0.00
5	4.36	4.36	0.00	4.46	4.45	0.02
6	3.72	3.73	−0.01	3.88	3.93	−0.04
7	4.09	4.08	0.01	4.20	4.20	0.00
9	4.39	4.39	0.00	4.48	4.48	0.00
10	4.17	4.17	0.00	4.35	4.36	−0.01
11	4.01	4.01	0.00	3.93	3.93	0.00
13	4.50	4.50	0.00	4.56	4.55	0.01
14	4.41	4.41	0.00	4.61	4.62	−0.01
15	4.53	4.54	−0.01	4.68	4.67	0.01
16	3.57	3.56	0.01	3.79	3.79	0.00
18	4.29	4.28	0.01	4.38	4.38	0.00
19	4.25	4.25	0.00	4.42	4.43	0.00
20	4.44	4.45	−0.01	4.64	4.64	0.00
B13	4.10	4.10	0.00	4.47	4.48	−0.01
Average			0.01			0.01

[a)]Experimental cytotoxic activity; [b)]predicted activity by the CoMSIA model with electrostatic, hydrophobic, and hydrogen bond acceptor fields; [c)]difference between the experimental and predicted activities; The pIC_{50} ($-\log IC_{50}$) values were converted from IC_{50} values.

Table 4. Residuals of the predicted cytotoxicities (pIC_{50}) of test set

Compounds	Prostate cancer cells (PC-3 cells)			Leukemia cells (HL-60 cells)		
	Experimental[a)]	Predicted[b)]	Residual[c)]	Experimental[a)]	Predicted[b)]	Residual[c)]
2	4.02	4.02	0.00	4.11	4.12	−0.01
8	4.19	4.17	0.02	4.35	4.34	0.01
12	4.28	4.27	0.01	4.26	4.23	0.03
17	4.12	4.21	−0.08	4.17	4.14	0.03
Average			0.03			0.02

[a)]Experimental cytotoxic activity; [b)]predicted activity by the CoMSIA model with electrostatic, hydrophobic, and hydrogen bond acceptor fields; [c)]difference between the experimental and predicted activities; The pIC_{50} ($-\log IC_{50}$) values were converted from IC_{50} values.

activities. The compounds with a 1R, 2R configuration (11, 12, 13, 14, and 15) were more active than corresponding compounds with other configurations. Compounds (11-20) with C_3-OH and a *para* nitro group in the phenyl ring had similar activities to the compounds (1-10) without these groups except for the compounds with a 1R, 2R configuration.

The cytotoxic activity in leukemia HL-60 cells was similar to that observed for prostate cancer PC-3 cells. The long alkyl chain compounds showed more potent cytotoxicity than the short alkyl chain compounds. Some of long alkyl chain ($C_{11}H_{23}$ and $C_{13}H_{27}$) analogues (4, 9, 14, 15, and 20) were more active than B13 with IC_{50} values of 28.5, 33.1, 24.7, 20.7, and 23 μM, respectively. The compounds with a 1R, 2R configuration (11, 12, 13, 14, and 15) produced more cytotoxicity than corresponding compounds with other configurations. Compounds (4, 9, 13, 14, 15, and 20) with a long alkyl chain showed more potent activities than B13 against both tumor cell lines.

3D-QSAR analysis

The statistical data for the CoMSIA model are summarized in Table 2. The residuals between the experimental and predicted cytotoxicity (pIC_{50}) are listed in Table 3 and 4, respectively.

Prostate cancer PC-3 cells

The PLS analysis of the CoMSIA model with electrostatic, hydrophobic, and hydrogen bond acceptor fields provided a cross-validated coefficient q^2 value of 0.816 and the non-cross-validated coefficient r^2 value of 0.999 with the optimum components number of 4, SEE of 0.009, and F value of 3841.601. The predictive ability of the model is expressed by the r^2_{pred} value, which is analogous to the cross-validated q^2, and the predicted r^2 value of this model was 0.776. The experimental pIC_{50} values, predicted pIC_{50} values, and the residuals for training and test sets are shown in Table 3 and 4, respectively. Fig. 2A describes the correlation between the experimental versus predicted pIC_{50} values for

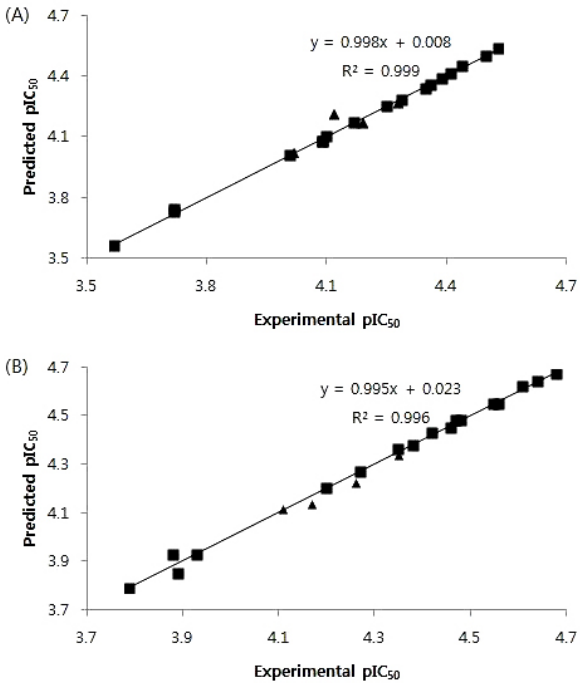

Fig. 2. Graph of the correlation between experimental and predicted activities for training and test set compounds. (A) Prostate cancer PC-3 cells. (B) Leukemia HL-60 cells. The IC_{50} values were transformed into pIC_{50} ($-\log IC_{50}$) values (■: training set compounds, ▲: test set compounds).

the training and test set compounds.

Leukemia HL-60 cells

The CoMSIA model with electrostatic, hydrophobic, and hydrogen bond acceptor fields gave the cross-validated q^2 value of 0.702, non-cross-validated r^2 value of 0.997, and PLS components of 4, respectively. With this model, the predicted r^2 value (r^2_{pred}) was 0.974 and the predicted pIC_{50} values and residuals of the training set and test set are presented in Table 3 and 4, respectively. The graph of experimental *versus* predicted pIC_{50} values for the training and test sets is shown in Fig. 2B.

DISCUSSION

In our *in vitro* biological assay, compound (15) showed strong activity against both prostate cancer PC-3 and leukemia HL-60 cells with IC_{50} values of 29.2 and 20.7 μM, respectively. The compounds with a $C_{13}H_{27}$ alkyl chain (5, 15, and 20) gave more potent cytotoxicity than B13, which also had a $C_{13}H_{27}$ alkyl chain, suggesting that the amide group of B13 could be replaced by a sulfonamide group to increase activity. This finding provides some clues to guide the design of new B13 analogues, since the sulfonamides are generally more water soluble and stable to hydrolysis by amidase than the amide compounds. The stereochemistry in the propyl group was not critical to biological activity, although the compounds with a 1R, 2R configuration (11, 12, 13, 14, and 15) showed more activity than corresponding compounds with other configurations. In general, compounds with long alkyl chains produced increased activity compared to compounds with short alkyl chains.

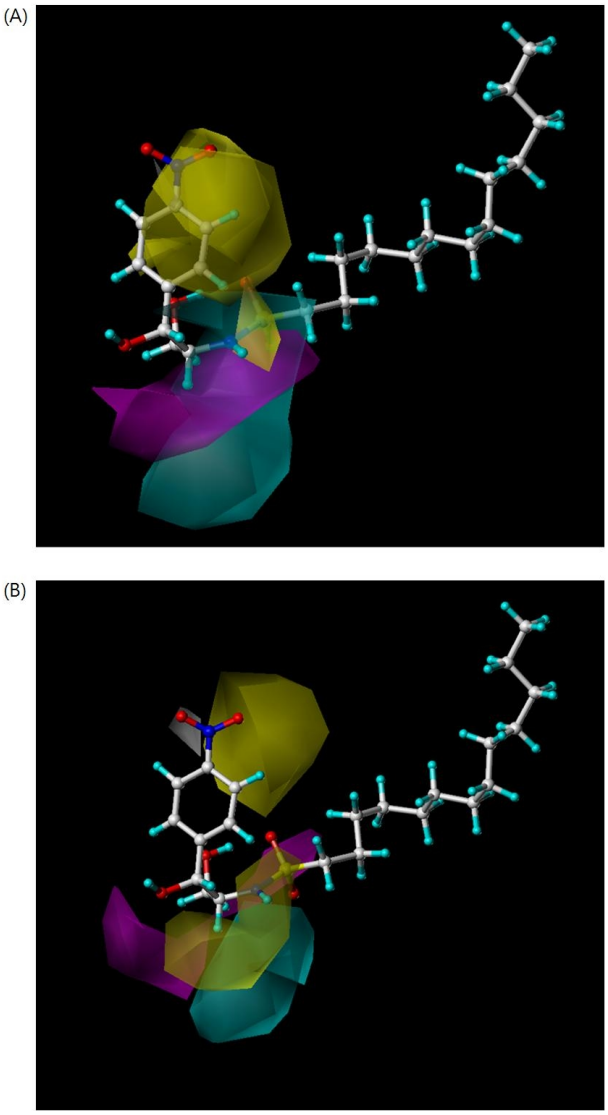

Fig. 3. 3D-contour maps of the CoMSIA models with electrostatic, hydrophobic, and hydrogen bond acceptor fields. (A) Prostate cancer PC-3 cells. (B) Leukemia HL-60 cells. Compound (15) is shown within the fields (blue, favorable electrostatic; red, unfavorable electrostatic; yellow, favorable hydrophobic; white, unfavorable hydrophobic; magenta, favorable hydrogen bond acceptor; cyan, unfavorable hydrogen bond acceptor).

For prostate cancer PC-3cells, the statistical data from the CoMSIA model showed a high cross-validated q^2 value (0.816) and non-cross-validated coefficient r^2 value (0.999). Its q^2 value, higher than 0.5, suggested that this model was predictive for validation. The corresponding field contributions of electrostatic (E), hydrophobic (H), and hydrogen-bond acceptor (A) were 41.6%, 33.5%, and 24.9%, respectively. In the CoMSIA model of leukemia HL-60 cells, good predictivity was represented by high q^2 (0.702) and r^2 (0.997) coefficient values. The electrostatic (51.8%), hydrophobic (25.4%), and hydrogen-bond acceptor field (22.8%) contributions indicate that electrostatic ligand-receptor in-

teractions are mainly involved in the cytotoxicity. The small average residual value (0.01) between experimental and predicted activities in Table 3 shows that the predicted activities from CoMSIA models are correlated well with the experimental activities. To validate the predictivity of CoMSIA models, the diverse configurations at C_1 and C_2 were selected for the test set and their small average residual values (0.03 and 0.02) indicate that both models are accurate to predict the cytotoxicity of the test set molecules (Table 4).

The CoMSIA 3D-contour maps were used to visualize the information of the derived 3D-QSAR models for PC-3 and HL-60 cells (Fig. 3). The maps use the characteristics of the compounds, which are important for biological activity and show the regions around molecules where increased or decreased activities are expected based on physicochemical property changes in the molecules. In an electrostatic contour map, the blue and red regions are favorable for positive and negative charges, respectively. The yellow contours indicate where hydrophobic groups (e.g. methyl and phenyl) increase biological activity, whereas the white contours show regions where hydrophilic groups (e.g., hydroxyl, carbonyl, and amino) increase activity. The magenta area favors a hydrogen bond acceptor (electronegative atoms such as fluorine, oxygen, and nitrogen), while the cyan represents an unfavorable region. The molecule in the contour maps is compound (15), which shows the most potent cytotoxicity.

The CoMSIA contour map of prostate cancer PC-3 cells (Fig. 3A) was similar to that of leukemia HL-60 cells (Fig. 3B). The contour map of PC-3 cells (Fig. 3A) revealed a blue contour at the NH and red contours near the oxygen atoms of the sulfonamide, which helps to explain the strong cytotoxic activity of compound (15). The yellow contours were shown at the *ortho* and *meta* positions of the phenyl ring, suggesting that the introduction of a naphthyl ring instead of phenyl ring or small alkyl group like CH_3 at these positions would increase activity. This finding was supported by the compounds (6, 11, and 16) in which yellow contours were superimposed with NO_2 or sulfonamide groups to give less potent activities. The yellow contours at the phenyl ring in compounds (4 and 9) and the white contours at NH moiety in compounds (15 and 20) provide clues about their high cytotoxicity. The magenta contour is near the oxygen atoms of the sulfonamide and the cyan contours were around the hydrogen atoms of the NH. These magenta and cyan contours appear in similar areas in compounds (4, 9, 13, and 20), thus explaining their high potency.

The contour map of HL-60 cells (Fig. 3B) displayed the blue contour at NH and red contours around the oxygen atoms of the sulfonamide, demonstrating the potent activity of the compound (15). The yellow contours were placed at the *meta* positions of the phenyl ring and C_2-H. The yellow contours appeared around the NO_2 or sulfonamide groups in compounds (6, 11, and 16) and the phenyl ring and methyl group in compounds (4 and 9) to explain low potency of the compounds (6, 11, and 16) and high potency of the compounds (4 and 9). The magenta contour was around the oxygen atoms of C_1-OH and the sulfonamide and cyan contours were near the hydrogen atoms of NH. In compounds (4, 9, 13, and 20), a similar distribution of magenta and cyan contours was found indicating their strong cytotoxicity.

In conclusion, compounds (4, 9, 13, 14, 15, and 20) gave more potent cytotoxicity than B13 in both tumor cell lines. The good predictivity of the CoMSIA models was explained by high q^2 (0.816 and 0.702) and r^2 (0.999 and 0.997) coefficient values. The low average residual values (training set for 0.01; test set for 0.03 and 0.02) in Table 3 and 4 indicate that the predicted activities from the CoMSIA models of PC-3 and HL-60 cell lines correlates well with the experimental activities. The cytotoxic assay and 3D-QSAR analysis suggested that the sulfonamide group, long alkyl chains, and 1R, 2R configuration are important for the cytotoxic activities. Moreover, our results suggest that the introduction of hydrophobic groups in the phenyl ring will increase the cytotoxicity.

ACKNOWLEDGEMENTS

This research was supported by Chung-Ang University Research Scholarship Grants in 2012.

REFERENCES

1. **Bionda C, Portoukalian J, Schmitt D, Rodriguez-Lafrasse C, Ardail D**. Subcellular compartmentalization of ceramide metabolism: MAM (mitochondria-associated membrane) and/or mitochondria? *Biochem J*. 2004;382:527-533.
2. **Futerman AH, Hannun YA**. The complex life of simple sphingolipids. *EMBO Rep*. 2004;5:777-782.
3. **Pettus BJ, Chalfant CE, Hannun YA**. Ceramide in apoptosis: an overview and current perspectives. *Biochim Biophys Acta*. 2002;1585:114-125.
4. **Carpinteiro A, Dumitru C, Schenck M, Gulbins E**. Ceramide-induced cell death in malignant cells. *Cancer Lett*. 2008;264: 1-10.
5. **Kim HJ, Song JY, Park HJ, Park HK, Yun DH, Chung JH**. Naringin protects against rotenone-induced apoptosis in human neuroblastoma SH-SY5Y cells. *Korean J Physiol Pharmacol*. 2009;13:281-285.
6. **Fillet M, Bentires-Alj M, Deregowski V, Greimers R, Gielen J, Piette J, Bours V, Merville MP**. Mechanisms involved in exogenous C2- and C6-ceramide-induced cancer cell toxicity. *Biochem Pharmaco*l. 2003;65:1633-1642.
7. **López-Marure R, Gutiérrez G, Mendoza C, Ventura JL, Sánchez L, Reyes Maldonado E, Zentella A, Montaño LF**. Ceramide promotes the death of human cervical tumor cells in the absence of biochemical and morphological markers of apoptosis. *Biochem Biophys Res Commun*. 2002;293:1028-1036.
8. **Ogretmen B, Pettus BJ, Rossi MJ, Wood R, Usta J, Szulc Z, Bielawska A, Obeid LM, Hannun YA**. Biochemical mechanisms of the generation of endogenous long chain ceramide in response to exogenous short chain ceramide in the A549 human lung adenocarcinoma cell line. Role for endogenous ceramide in mediating the action of exogenous ceramide. *J Biol Chem*. 2002;277:12960-12969.
9. **Bedia C, Triola G, Casas J, Llebaria A, Fabriàs G**. Analogs of the dihydroceramide desaturase inhibitor GT11 modified at the amide function: synthesis and biological activities. *Org Biomol Chem*. 2005;3:3707-3712.
10. **Gouazé V, Liu YY, Prickett CS, Yu JY, Giuliano AE, Cabot MC**. Glucosylceramide synthase blockade down-regulates P-glycoprotein and resensitizes multidrug-resistant breast cancer cells to anticancer drugs. *Cancer Res*. 2005;65:3861-3867.
11. **Granot T, Milhas D, Carpentier S, Dagan A, Ségui B, Gatt S, Levade T**. Caspase-dependent and -independent cell death of Jurkat human leukemia cells induced by novel synthetic ceramide analogs. *Leukemia*. 2006;20:392-399.
12. **Grijalvo S, Bedia C, Triola G, Casas J, Llebaria A, Teixidó J, Rabal O, Levade T, Delgado A, Fabriàs G**. Design, synthesis and activity as acid ceramidase inhibitors of 2-oxooctanoyl and N-oleoylethanolamine analogues. *Chem Phys Lipids*. 2006;144: 69-84.

13. **Morales A, París R, Villanueva A, Llacuna L, García-Ruiz C, Fernández-Checa JC**. Pharmacological inhibition or small interfering RNA targeting acid ceramidase sensitizes hepatoma cells to chemotherapy and reduces tumor growth *in vivo*. *Oncogene*. 2007;26:905-916.
14. **Dindo D, Dahm F, Szulc Z, Bielawska A, Obeid LM, Hannun YA, Graf R, Clavien PA**. Cationic long-chain ceramide LCL-30 induces cell death by mitochondrial targeting in SW403 cells. *Mol Cancer Ther*. 2006;5:1520-1529.
15. **Senkal CE, Ponnusamy S, Rossi MJ, Sundararaj K, Szulc Z, Bielawski J, Bielawska A, Meyer M, Cobanoglu B, Koybasi S, Sinha D, Day TA, Obeid LM, Hannun YA, Ogretmen B**. Potent antitumor activity of a novel cationic pyridinium-ceramide alone or in combination with gemcitabine against human head and neck squamous cell carcinomas *in vitro* and *in vivo*. *J Pharmacol Exp Ther*. 2006;317:1188-1199.
16. **Granot T, Milhas D, Carpentier S, Dagan A, Ségui B, Gatt S, Levade T**. Caspase-dependent and -independent cell death of Jurkat human leukemia cells induced by novel synthetic ceramide analogs. *Leukemia*. 2006;20:392-399.
17. **Nam EJ, Lee HS, Lee YJ, Joo WS, Maeng S, Im HI, Park CW, Kim YS**. Ceramide is involved in MPP+ -induced cytotoxicity in human neuroblastoma cells. *Korean J Physiol Pharmacol*. 2002;6:281-286.
18. **Ahn EH, Schroeder JJ**. Induction of apoptosis by sphingosine, sphinganine, and C(2)-ceramide in human colon cancer cells, but not by C(2)-dihydroceramide. *Anticancer Re*s. 2010;30:2881-2884.
19. **Chun YJ, Lee S, Yang SA, Park S, Kim MY**. Modulation of CYP3A4 expression by ceramide in human colon carcinoma HT-29 cells. *Biochem Biophys Res Commun*. 2002;298:687-692.
20. **Macchia M, Barontini S, Bertini S, Di Bussolo V, Fogli S, Giovannetti E, Grossi E, Minutolo F, Danesi R**. Design, synthesis, and characterization of the antitumor activity of novel ceramide analogues. *J Med Chem*. 2001;44:3994-4000.
21. **Oh JE, So KS, Lim SJ, Kim MY**. Induction of apoptotic cell death by a ceramide analog in PC-3 prostate cancer cells. *Arch Pharm Res*. 2006;29:1140-1146.
22. **Szulc ZM, Mayroo N, Bai A, Bielawski J, Liu X, Norris JS, Hannun YA, Bielawska A**. Novel analogs of D-e-MAPP and B13. Part 1: synthesis and evaluation as potential anticancer agents. *Bioorg Med Chem*. 2008;16:1015-1031.
23. **Alphonse G, Bionda C, Aloy MT, Ardail D, Rousson R, Rodriguez-Lafrasse C**. Overcoming resistance to gamma-rays in squamous carcinoma cells by poly-drug elevation of ceramide levels. *Oncogene*. 2004;23:2703-2715.
24. **Lépine S, Lakatos B, Courageot MP, Le Stunff H, Sulpice JC, Giraud F**. Sphingosine contributes to glucocorticoid-induced apoptosis of thymocytes independently of the mitochondrial pathway. *J Immunol*. 2004;173:3783-3790.
25. **Maupas-Schwalm F, Augé N, Robinet C, Cambus JP, Parsons SJ, Salvayre R, Nègre-Salvayre A**. The sphingomyelin/ceramide pathway is involved in ERK1/2 phosphorylation, cell proliferation, and uPAR overexpression induced by tissue-type plasminogen activator. *FASEB J*. 2004;18:1398-1400.
26. **Rodriguez-Lafrasse C, Alphonse G, Aloy MT, Ardail D, Gerard JP, Louisot P, Rousson R**. Increasing endogenous ceramide using inhibitors of sphingolipid metabolism maximizes ionizing radiation-reduced mitochondrial injury and apoptotic cell killing *Int. J Cancer*. 2002;101:589-598.
27. **Raisova M, Goltz G, Bektas M, Bielawska A, Riebeling C, Hossini AM, Eberle J, Hannun YA, Orfanos CE, Geilen CC**. Bcl-2 overexpression prevents apoptosis induced by ceramidase inhibitors in malignant melanoma and HaCaT keratinocytes. *FEBS Lett*. 2002;516:47-52.
28. **Samsel L, Zaidel G, Drumgoole HM, Jelovac D, Drachenberg C, Rhee JG, Brodie AM, Bielawska A, Smyth MJ**. The ceramide analog, B13, induces apoptosis in prostate cancer cell lines and inhibits tumor growth in prostate cancer xenografts. *Prostate*. 2004;58:382-393.
29. **Selzner M, Bielawska A, Morse MA, Rüdiger HA, Sindram D, Hannun YA, Clavien PA**. Induction of apoptotic cell death and prevention of tumor growth by ceramide analogues in metastatic human colon cancer. *Cancer Res*. 2001;61:1233-1240.
30. **Samsel L, Zaidel G, Drumgoole HM, Jelovac D, Drachenberg C, Rhee JG, Brodie AM, Bielawska A, Smyth MJ**. The ceramide analog, B13, induces apoptosis in prostate cancer cell lines and inhibits tumor growth in prostate cancer xenografts. *Prostate*. 2004;58:382-393.
31. **Holman DH, Turner LS, El-Zawahry A, Elojeimy S, Liu X, Bielawski J, Szulc ZM, Norris K, Zeidan YH, Hannun YA, Bielawska A, Norris JS**. Lysosomotropic acid ceramidase inhibitor induces apoptosis in prostate cancer cells. *Cancer Chemother Pharmacol*. 2008;61:231-242.
32. **Usta J, El Bawab S, Roddy P, Szulc ZM, Yusuf, Hannun A, Bielawska A**. Structural requirements of ceramide and sphingosine based inhibitors of mitochondrial ceramidase. *Biochemistry*. 2001;40:9657-9668.
33. **Boyd AE 3rd**. Sulfonylurea receptors, ion channels, and fruit flies. *Diabetes*. 1988;37:847-850.
34. **Maren TH**. Relatons between structure and biological activity of sulfonamides. *Annu Rev Pharmacol Toxicol*. 1976;16:309-327.
35. **Abbate F, Casini A, Owa T, Scozzafava A, Supuran CT**. Carbonic anhydrase inhibitors: E7070,a sulfonamide anticancer agent, potently inhibits cytosolic isozymes I and II, and transmembrane, tumor-associated isozyme IX. *Bioorg Med Chem Lett*. 2004;14:217-223.
36. **Rostom SA**. Synthesis and in vitro antitumor evaluation of some indeno[1,2-c]pyrazol(in)es substituted with sulfonamide, sulfonylurea(-thiourea) pharmacophores, and some derived thiazole ring systems. *Bioorg Med Chem*. 2006;14:6475-6485.
37. **Kim YJ, Kim EA, Sohn UD, Yim CB, Im C**. Cytotoxic Activity and Structure Activity Relationship of Ceramide Analogues in Caki-2 and HL-60 Cells. *Korean J Physiol Pharmacol*. 2010;14:441-447.
38. **Park SM**. Synthesis and anti-cancer activity of alkylsulfone amide derivatives. Chung-Ang Graduate School Master Thesis. 2002.
39. **Park JG, Kramer BS, Steinberg SM, Carmichael J, Collins JM, Minna JD, Gazdar AF**. Chemosensitivity testing of human colorectal carcinoma cell lines using a tetrazolium-based colorimetric assay. *Cancer Res*. 1987;47:5875-5879.
40. **SYBYL Molecular Modeling Software**. St. Louis, USA: Tripos Inc; 2012.